Available online at www.sciencedirect.com
ScienceDirect
Journal of Power Sources 179 (2008) 9–16
JOURNAL OF POWER SOURCES
www.elsevier.com/locate/jpowsour

Performance and stability of composite nickel and molybdenum sulfide-based anodes for SOFC utilizing H_2S

V. Vorontsov, W. An, J.L. Luo *, A.R. Sanger, K.T. Chuang

Department of Chemical and Materials Engineering, University of Alberta, Edmonton, Alberta T6G 2G6, Canada

Received 5 December 2007; received in revised form 28 December 2007; accepted 31 December 2007
Available online 4 January 2008

Abstract

Performances of four anode compositions with different weight ratios of $Ni_{3\pm x}S_2$ to MoS_2 (2:1, 1:1, 1:2 and 1:4) were compared for H_2S oxidation in SOFC at 700–850 °C. Their thermal and chemical stability were determined using DSC/TGA, XRD, SEM and NAA. Electrochemical stability was investigated in fuel cell mode under OCV and constant overpotential conditions. It was shown that MoS_2 disappearance previously attributed to its volatility at temperature above 450 °C was instead related to its preliminary oxidation to MoO_3 in fuel cell mode as MoO_3 is highly volatile at temperatures above 600 °C. Suppression of volatility of MoO_3 by addition of $Ni_{3\pm x}S_2$ was shown by DSC/TGA analysis. Highest power density ca. 300 mW cm^2 at 850 °C was achieved with 1:1 weight ratio anode composition. All four compositions had unstable electrochemical performance which was more pronounced under polarization conditions than at OCV.

Keywords: Hydrogen sulfide; Nickel sulfide; Molybdenum sulfide; Solid oxide fuel cell

1. Introduction

Each year large amounts of H_2S are generated worldwide, mostly as by-products from petroleum, natural gas and coal gasification industries. The adverse effects of H_2S on industrial processes, human health and the environment make it necessary to remove it from all effluent streams. It is anticipated that additional large quantities of H_2S will be produced due to an increase in utilization of high-sulfur crude oils and an expansion of coal gasification/liquefaction technology.

Many processes have been developed to remove and/or recover H_2S, including adsorption, absorption, hydrogen production and conversion to elemental sulfur via the two-step Claus process. Such H_2S processing units require high capital investments. Also, as the final products are of low commercial value, there is high demand to find more economical and efficient hydrogen sulfide recovery methods.

It is well known that H_2S decomposes at high temperatures into hydrogen and sulfur via the general equilibrium reaction (Eq. (1)):

$$H_2S \leftrightarrow 1/2S_2 + H_2 \quad (1)$$

Therefore, it would be highly desirable if hydrogen originating from this reaction could be electrochemically oxidized in a SOFC to generate electrical energy, leaving sulfur and water as exclusive anode reaction products. Thus utilization of H_2S in solid oxide fuel cells provides a potentially economical and powerful alternative for concurrent chemical conversion and power generation.

The feasibility of an electrochemical oxidation of H_2S in SOFC was first demonstrated in the late 1980s. Pujare et al. had showed that SOFC based on yttria-stabilized zirconia (YSZ) electrolyte could operate on high levels of H_2S fuel at 900 °C [1]. Subsequent studies by the same group revealed that various thiospinels and transition metal sulfides were active as anode electrocatalysts for H_2S oxidation [2]. Among many materials studied, $NiFe_2S_4 > WS_2 > CuCo_2S_4$ (in order of decreasing activity) anodes were the most active. Despite reported high values of the activity for H_2S oxidation, there were no reports of analysis of stability of such materials under fuel cell conditions.

Ong et al. studied anodic oxidation of H_2 and H_2S on YSZ electrolyte with porous Au, Ni and Pt electrodes [3]. They

* Corresponding author. Tel.: +1 780 492 2232; fax: +1 780 492 2881.
E-mail address: jingli.luo@ualberta.ca (J.L. Luo).

0378-7753/$ – see front matter © 2008 Elsevier B.V. All rights reserved.
doi:10.1016/j.jpowsour.2007.12.097

showed that, although Au is not a highly active oxidation catalyst, it has the advantage that it is not susceptible to poisoning. Ni and Pt anodes had high initial performance but experienced an abrupt drop in performance attributable to the reversible formation of NiS and PtS at the anode surface. Although these metallic sulfide phases are electronically conductive, the sulfidation process causes the delamination of the anode material from YSZ electrolyte.

The potential for utilization of H_2S in ceria-based SOFC with porous platinum electrodes has also been demonstrated by Winnick and Weaver [4]. However, while doped ceria exhibited higher ionic conductivities than YSZ, the electronic conductivity of ceria at high temperatures in a H_2S-rich environment reduced the open circuit potential, thus leading to decrease in cell power density. Later results from the same group showed the performance of a SOFC utilizing thin 40 μm YSZ electrolyte and Li_2S/CoS anode with initial powder density to be ca. 400 mW cm^{-2} at 770 °C. Stability tests performed with this material showed that it is thermally unstable and cell performance decreased with time [5].

Our group has previously investigated fuel cell performances using $Ni_{3\pm x}S_2$, CoS, MoS_2 and their combinations as anode materials at 700–850 °C [6–8]. MoS_2 mixed with $Ni_{3\pm x}S_2$ in a 1:1 weight ratio showed the highest activity with maximum power density ca. 40 mW cm^{-2} at 850 °C in [H_2S, $Ni_{3\pm x}S_2$–MoS_2/YSZ/Pt, air] fuel cell configuration. We have also developed proprietary formulations with superior performance by mechanically mixing these composite sulfides with Ag and YSZ powders to improve conductivity and electrochemical reaction volume [8]. A power density of 200 mW cm^{-2} was achieved at 850 °C in [H_2S, $Ni_{3\pm x}S_2$–MoS_2–Ag–YSZ/YSZ/Pt, air] fuel cell configuration.

The aim of the present work was to investigate performance and stability of MoS_2 and $Ni_{3\pm x}S_2$-based anodes with different weight ratios of nickel to molybdenum sulfides to find optimum anode composition for SOFC operating on pure H_2S at 700–850 °C.

2. Experimental

2.1. Preparation of anode materials

The sources of metal sulfides used as starting materials for anode catalyst preparation were MoS_2 (Aldrich, 99.9%) and nickel sulfide (Alfa Aesar, 99.9%). A range of $Ni_{3\pm x}S_2$–MoS_2 catalysts was prepared using different initial nickel sulfide to MoS_2 ratios by weight (1:1, 1:2, 1:4 and 2:1) as shown in Table 1. All catalysts were admixed with 5 wt% of Ag (<325 mesh) and 5 wt% of YSZ (10–20 μm) powders (both from Alfa Aesar). All resulting powders were mixed and homogenized in 95% ethanol in an ultrasonic bath for several hours. All formulations were heat treated at 1050 °C for 2 h under N_2 stream (99.9995% purity, from Praxair). The resulting powders were then re-ground before use in preparation of electrode/electrolyte assemblies.

2.2. Cell design

Commercially available 8 mol% yttria-stabilized zirconia (YSZ-8) disks were obtained from Intertec Southwest for use as the electrolyte. Disks were 0.3 mm thick and 25.4 mm in diameter. To enhance the adhesion between the electrode material and the YSZ disk, the surfaces of the electrolytes were manually roughened by mechanical grinding using silicon carbide powder then cleaned. Platinum paste (Heraeus CL11-5100) was screen printed onto one side of the electrolyte disk as cathode. Anode catalyst powders were mixed with α-terpineol to make a paste which then was screen printed onto the other side of YSZ disk. After drying overnight at room temperature, disks were fired at 1050 °C for 30 min in N_2 flow to achieve good adhesion of electrodes to the membrane. The anode and cathode each had a geometrical area ca. 1 cm^2 and were ca. 50 μm thick.

2.3. Experimental setup

The experimental setup is described in Ref. [9]. In brief, the resulting membrane electrode assembly (MEA) was sandwiched between two pairs of co-axially aligned pairs of alumina cylinders. The inner cylinders served as anode and cathode feed and the outer ones as exhaust, respectively. The outer perimeter of each tube was sealed to the respective rims of the membrane electrode assembly by applying a thin layer of ceramic adhesive (Aremco 503). The whole operating section of the assembly was placed in a tubular furnace (Thermolyne F79300), while the ends of the alumina cylinders extended outside the furnace to allow connections for feed and exhaust gases. The furnace had a uniform temperature zone (±0.6 °C) over the central 7.62 cm length of the cell. The ceramic sealant was cured using the manufacture's recommended procedure while high purity N_2 (99.9995%) and extra dry air flowed through the respective anode and cathode chambers. The cell assembly was leak tested prior to operation of the cell under reaction conditions. Experiments were conducted in the temperature range of 700–850 °C and, after the temperature stabilized, flow rates of H_2S 25 cm^3 min^{-1} and air 50 cm^3 min^{-1} were introduced to anode and cathode sides of the membrane assembly, respectively. Gold gauze (52 mesh) was used as current collector for

Table 1
Weight % of Ni and Mo determined by neutron activation analysis (NAA)[a]

NiS to MoS_2 by weight (theoretical)	2:1		1:1		1:2		1:4	
	Ni	Mo	Ni	Mo	Ni	Mo	Ni	Mo
Before fuel cell test (wt%)	42.5 ± 0.6	19.9 ± 0.6	37.8 ± 0.7	23.6 ± 0.2	20.4 ± 0.6	38.3 ± 0.3	12.1 ± 0.6	42.2 ± 0.4
After fuel cell test (wt%)	41.0 ± 0.9	19.4 ± 0.2	35.4 ± 0.6	23.7 ± 0.2	23.7 ± 0.8	40.5 ± 0.4	13.6 ± 0.6	31.1 ± 0.5

[a] Anode catalyst composition by weight: 90% MoS_2–$Ni_{3\pm x}S_2$; 5% Ag; 5% YSZ.

both electrodes since it is more stable in H_2S [10–12] than Pt [13–15]. The gold gauzes were in intimate contact with the surface of each electrode and other sides were spot welded to gold lead wires.

2.4. Electrochemical characterization

All electrochemical measurements where performed when the anode feed was switched to H_2S and a stable open circuit voltage (OCV) was established. Fuel cells' potentiodynamic and potentiostatic characteristics were recorded using a Solartron electrochemical interface SI 1287 system. Electrochemical impedance spectroscopy (EIS) measurements were performed at OCV with the applied amplitude 10 mV over the frequency range 100 kHz to 0.1 Hz using a Solartron 1255B frequency response analyzer.

2.5. Anode material characterization

Weight change and thermal stability of anode materials over the temperature range 25–1000 °C were determined using simultaneous differential scanning calorimetry (DSC) and thermogravimetry (TGA) analyses using a NETZSCH STA 409PC system under N_2 or air flows and a temperature ramp of 10 °C min^{-1}. Images and composition of fresh and used anodes were obtained using scanning electron microscopy with X-ray energy dispersive analysis (SEM–EDX) using a Hitachi S-2700 scanning electron microscope equipped with a PGT IMIX digital imaging system and a PGT PRISM IG detector for EDX. Phase composition and chemical stability were analyzed using X-ray diffraction (XRD) with a Rigaku Rotaflex X-ray diffractmeter. Relative concentrations of Ni and Mo in prepared catalyst powders before and after fuel cell test were obtained using neutron activation analysis (NAA) at the SLOWPOKE Nuclear Reactor Facility.

3. Results and discussion

3.1. Thermal and chemical stability of MoS_2, $Ni_{3\pm x}S_2$ and a mixture of $MoS_2/Ni_{3\pm x}S_2$

MoS_2 is most commonly used for hydrodesulfurization processes in the temperature range 300–400 °C and as a catalyst for hydrogen production from hydrogen sulfide at 600–800 °C [16,17]. Because of its high electronic conduction, MoS_2 could be a good candidate as an anode material in H_2S-powered SOFC. Our group had determined the performance of MoS_2 as an anode material for H_2S-powered SOFC [6,7]. However, the fuel cell performance results with MoS_2 anode were relatively low. Moreover, there was little or no MoS_2 left on YSZ disks after several hours of operation at 850 °C [6,7], although we have sintered the MoS_2 with the YSZ electrolyte with no visual changes and the XRD results confirmed that there were no chemical or phase changes in N_2 at 1050 °C. The disappearance of MoS_2 was previously attributed to volatility of MoS_2.

Some controversy exists on stability of MoS_2. Some sources described MoS_2 as volatile at temperatures above 450 °C [6,7], while others stated that it decomposes at 650 °C and above [12]. Other sources reported MoS_2 to be thermally and chemically stable in vacuum, inert and reducing atmospheres up to 1100 °C [18–22]. It is well known that MoS_2 is stable in H_2S at least up 800 °C [16,17]. Therefore, we did not expect any volatility or decomposition during fuel cell performance. If there was no volatilization of MoS_2 under H_2S, the only time when an unwanted reaction could happen to the anode material was during fuel cell heating to 700 °C under N_2, before the anode feed was switched to H_2S. Indeed, when the cell was heated to 700 °C and then cooled down to room temperature under N_2 flow, without any H_2S flow in between, the anode surface appeared to have oxidized since its color changed to orange–yellow, characteristics of MoO_x. Thus MoS_2 was susceptible to oxidation to volatile MoO_3 by trace amounts of O_2 present during preparation for testing. To confirm the reason for the disappearance of MoS_2, thermal behavior for MoS_2 in N_2 atmosphere was investigated using TGA and DSC analyses and the results are shown in Fig. 1. The main feature of the TGA curve for MoS_2 is the absence of any weight change up to 1000 °C. Since XRD data of fresh and after-exposed MoS_2 samples did not show any major crystallographic differences, and there was no weight change upon exposure to N_2, we confirmed that MoS_2 is thermally stable and non-volatile in N_2 up to 1000 °C. Several peaks on the DSC curve are attributable to reversible phase transitions which are not necessarily accompanied by weight change (e.g., polymorphism or melting, etc.). We could not relate these peaks to MoS_2 phase diagram and there were no published sources on DSC for pure MoS_2 in N_2.

We investigated two possible sources of oxygen which could account for MoS_2 loss during fuel cell test preparation. First, some molecular oxygen could have leaked through sealant or crossover from the cathode side and oxidize MoS_2 to MoO_3. MoS_2 is readily oxidized at temperatures as low as 100 °C [23]. MoO_3 is a highly volatile compound with vapor pressure as high as 10.13 Pa at 661 °C in air, which increases very rapidly at high temperature [24]. This possibility was ruled out since YSZ disks with MoS_2 as anode electrocatalyst showed high and stable values of OCV (ca. 1.05 V) in the fuel cell mode which would be reduced and/or unstable if there were substantial oxygen leaks.

The second possible source was that there was an oxygen potential gradient across the YSZ membrane in the fuel cell setup in the heat up stage at which air on cathode side and N_2 on anode side which is switched to H_2S at 700 °C. An ideal electrolyte is one in which the only means for oxygen conveyance to the anode compartment is as oxide ions. In this case the chemical potential of oxygen is balanced by the electrical potential developed across electrolyte resulting in the zero net oxygen flux. However, YSZ also has small electronic conductivity, so there will be a small countercurrent of oxygen ion and electron fluxes which are related by the ratio of their respective conductivities in YSZ at any given temperature. The existence of the oxygen flux is responsible for the phenomena known as non-Faradaic electrochemical modification of catalytic activity (NEMCA) when the number of moles of species reacted is much higher than that proportional to the current [25]. According to Vayenas et al. [26], NEMCA is due to electrocatalytically driven

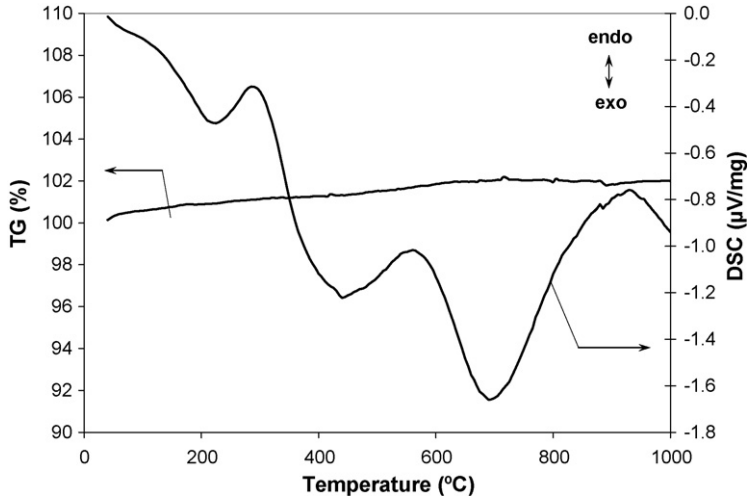

Fig. 1. TGA and DSC analysis of MoS_2 powder in N_2 atmosphere.

and controlled back-spillover of ions from solid electrolyte onto gas-exposed electrode surface. Under these conditions the two half-cell reactions taking place on cathode and anode will be reduction of oxygen (Eq. (2)) and oxidation of oxide ions (Eq. (3)), respectively, with a zero net reaction:

$$O_2 + 4e^- = 2O^{2-} \quad (2)$$

$$2O^{2-} = O_2 + 4e^- \quad (3)$$

Any oxygen so formed at the MoS_2 anode would oxidize the catalyst to MoO_3 even before H_2S is switched on. Even though O_2 concentration is low on the anodic side in N_2 stream it is highly active and easily reacts with the anode, leading to oxidation of MoS_2. Thus the small current of oxygen ions from the cathode under OCV conditions may explain why there was almost no MoS_2 left after testing and why the anode changed to a color characteristic of MoO_x. MoS_2 oxidized to MoO_3 in fuel cell during startup and MoO_3 is highly volatile at temperatures above 600 °C.

In contrast, there was no loss of Mo when composite MoS_2 and $Ni_{3\pm x}S_2$ were successfully used as SOFC anodes [6–8], and these anodes have shown much better electrochemical fuel cell performance than MoS_2. No volatility or color/phase changes were observed either visually or by XRD [8] when comparing fresh and used catalysts. In order to determine the effect of nickel sulfide on volatility and oxidative behavior of MoS_2, we performed thermal analysis of samples of pure sulfides and samples comprising MoS_2 mixed with $Ni_{3\pm x}S_2$ in 1:1 weight ratio in an air stream (Fig. 2).

MoS_2 showed initial mass loss at 450–550 °C. The mass diminished by 8.7%, a value close to that for conversion of all MoS_2 to MoO_3. The rapid drop, occurring as the temperature increased by only 100 °C, indicated that the transition took place in a single step, in agreement with the literature on MoS_2 oxidation [23]. In the temperature range 760–820 °C another rapid drop in weight (ca. 63%) occurred, attributable to sublimation of MoO_3. Weight loss continued after 860 °C at a slower rate, and after 950 °C it leveled off slowly. Endothermic peaks on the DSC curve shown in Fig. 3 corresponded to both weight-loss

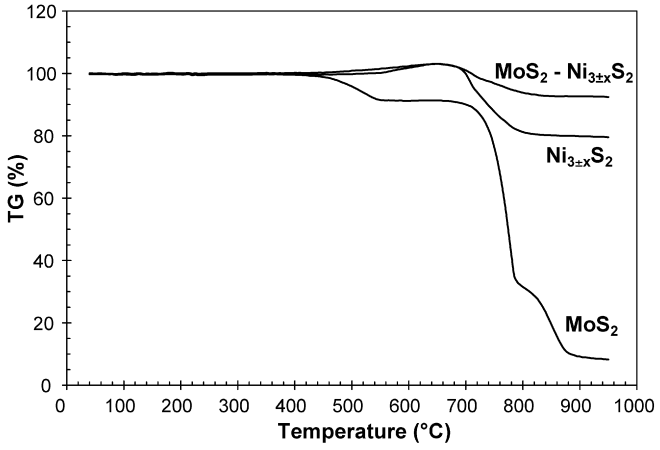

Fig. 2. TGA analysis of pure $Ni_{3\pm x}S_2$, MoS_2 and mixture of both in 1:1 weight ratio in air.

steps. The residual mass after heating was ca. 8%. Upon cooling to room temperature no change in mass is observed. Since MoO_3 is volatile above 600 °C one would expect mass change on cooling as well at least until sample is above 600 °C. Since

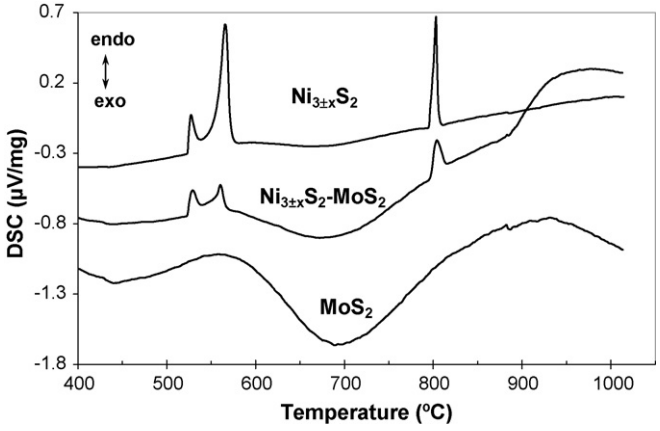

Fig. 3. DSC analysis of $Ni_{3\pm x}S_2$, MoS_2 and mixture of both in 1:1 weight ratio in N_2.

this was not observed it follows that this residual material left was not MoO_3 but something else like molybdenum oxysulfate or molybdenum dioxide. There was too little amount of sample left to run post-test XRD analysis on it.

$Ni_{3\pm x}S_2$ oxidation behavior varies substantially depending on sulfur content, heating rate and sample grain size [27,28]. Several reaction pathways are possible, with partial or complete oxidation of the initial nickel sulfide. The TGA curve for $Ni_{3\pm x}S_2$ sample showed a slight weight increase (ca. 3%) at 550–650 °C, followed by ca. 23% decrease in weight over the interval 650–800 °C. The XRD results have shown that the commercial $Ni_{3\pm x}S_2$ consisted mainly of Ni_3S_2 phase, but it is possible that either some amorphous or below-detectable XRD limit phases also were present. NAA results show Ni content in the sample as 70.3 wt%, which is too small for the Ni_3S_2 phase and too high for the NiS phase. According to the nickel–sulfur phase diagram [29], 70.3 wt% of Ni corresponds to a solid solution of Ni_3S_2 and Ni_7S_6 phases. The XRD analysis has shown the final oxidation product to be NiO.

We compared oxidation of composite nickel–molybdenum sulfides with the single phase materials. A mixture of $Ni_{3\pm x}S_2$ and MoS_2 showed an initial slight weight increase, similar to that observed for pure nickel sulfide, followed by a 7.7% weight decrease when compared with initial sample weight. Unlike the behavior of pure MoS_2, there was no rapid or substantial weight decrease for the mixture up to 1000 °C, and no change upon cooling the sample to room temperature in air. The XRD analysis has shown the existence of a single $NiMoO_4$ phase. No other phases such as MoO_3 or NiO have been detected, in contrast to products from oxidation of the corresponding single sulfides. Therefore, the addition of nickel sulfide prevents formation of MoO_3 from oxidation of MoS_2 that takes place *in situ* before the SOFC test. If one was to use 1:1 weight ratio of Ni_3S_2 to MoS_2 as the starting material composition then an 8.95% weight loss would be expected. This value is quite close to that (7.7%) obtained from the experimental TG curve. The difference between the values is attributed in large part to the presence of small amounts of phases other than Ni_3S_2 in the starting $Ni_{3\pm x}S_2$ material.

3.2. Stability of microstructures for pure $Ni_{3\pm x}S_2$ and a composite MoS_2–$Ni_{3\pm x}S_2$ anode

For successful application of a fuel cell anode, densification must be prevented to facilitate fast reactant–product mass transfer within a porous anode structure and to sustain high interfacial surface area. It was important to investigate thermal stability of the macrostructures of pure $Ni_{3\pm x}S_2$ and composite MoS_2–$Ni_{3\pm x}S_2$ anodes. DSC results for nickel sulfide heated in N_2 to 1000 °C are shown in Fig. 3. For pure nickel sulfide there were three characteristic sharp peaks and several smaller peaks. Two of these close endothermic peaks, at 564 °C and 524 °C, represented formation of $\beta_1(Ni_3S_2)$ from low temperature $\beta'(Ni_3S_2)$ phase; and $\beta_2(Ni_4S_3)$ phase which is formed by the reaction of $\beta'(Ni_3S_2)$ and $\gamma(Ni_7S_6)$ phases. Both β_1 and β_2 phases are stable only at temperatures higher than 500 °C, and they revert to $\beta'(Ni_3S_2)$ and $\gamma(Ni_7S_6)$ phases upon cooling below 500 °C. Reversibility was confirmed by doing two consecutive heating and cooling cycles in TG/DSC where the same behavior was observed in both case. Results coincide well with the nickel–sulfur phase diagram [29] and XRD showed existence of only $\beta'(Ni_3S_2)$ phase before and after heat treatment. A third sharp peak at 800–805 °C, which was not associated with a weight change, corresponded to melting of Ni_3S_2, which after cooling the sample was completely fused. The phase diagram shows existence of a melting point at ca. 800 °C. Thus results for the commercial material agreed well with the nickel–sulfur phase diagram [29]. Our results, together with some other literature reports [12], suggested that $Ni_{3\pm x}S_2$ alone was not a suitable anode material for SOFC operating at 700–850 °C since the material was susceptible to either excessive sintering or melting.

The DSC profile of composite MoS_2–$Ni_{3\pm x}S_2$ anode catalyst (1:1 weight ratio) (Fig. 3) showed a combination of peaks corresponding to those of the individual components. Although one peak was still present at ca. 800 °C, at a temperature similar to that attributed to the melting point of $Ni_{3\pm x}S_2$, there was no visible evidence of melting during the test of the composite anode. Similar results were reported for thermal decomposition of hydrogen sulfide over $Ni_{3\pm x}S_2$ catalyst, which had stable performance, and there was no decrease in surface area when the catalyst was mixed with Al_2O_3 or MoS_2 [30].

Although addition of $Ni_{3\pm x}S$ stabilized the composite catalyst against loss of Mo resulting from oxidation and improved fuel cell performance compared with that of MoS_2 alone, it was unknown whether the low thermal stability of nickel sulfide in the fuel cell operating temperature would affect performance over time. Consequently we determined fuel cell performance and stability using anode catalysts having different weight ratios of $Ni_{3\pm x}S_2$ to MoS_2 to find an optimal anode composition.

3.3. Fuel cell performance and stability using composite MoS_2–$Ni_{3\pm x}S_2$ anodes

Addition of 5 wt% each of Ag and YSZ powders increases electrochemical fuel cell performance, because of an increase in electronic conductivity due to the presence of Ag and an increase in the ionic conduction due to YSZ and an increase in triple phase boundaries [8]. Consequently, all our anode compositions under study were admixed with 5 wt% each of Ag and YSZ.

Fig. 4 presents impedance spectra for $Ni_{3\pm x}S_2$–MoS_2–Ag–YSZ anodes with different nickel sulfide to molybdenum sulfide weight ratios. At least two processes are seen to dominate in the EIS spectra at high (1–2 kHz) and low (1–10 Hz) frequencies. The spectra may contain contributions from more than two overlapping rate-limiting steps. We now have determined the contribution of ohmic (R_s) and total polarization (R_p) resistances. R_s is obtained as the high frequency intercept of the impedance with the Z' real axis, and R_p is the difference between the intercept of the impedance with the Z' real axis at the limit $f \rightarrow 0$ and the high frequency intercept. It can be seen that the fuel cell employing highest nickel sulfide content (Ni:Mo sulfides in 2:1 weight ratio) had the lowest ohmic resistance, but its polarization resistance was high compared with those of the 1:2 and 1:1 compositions. Total resistance (ohmic plus polarization)

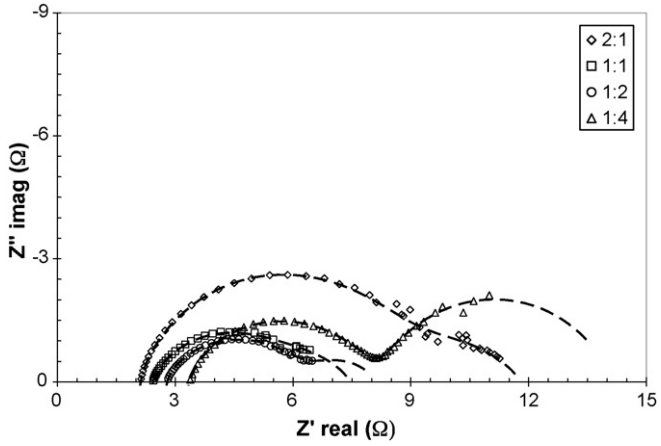

Fig. 4. EIS spectra of SOFC utilizing different weight ratios of $Ni_{3\pm x}S_2$ to MoS_2 in composite anode material at 850 °C (legend shows weight ratios of nickel to molybdenum sulfides).

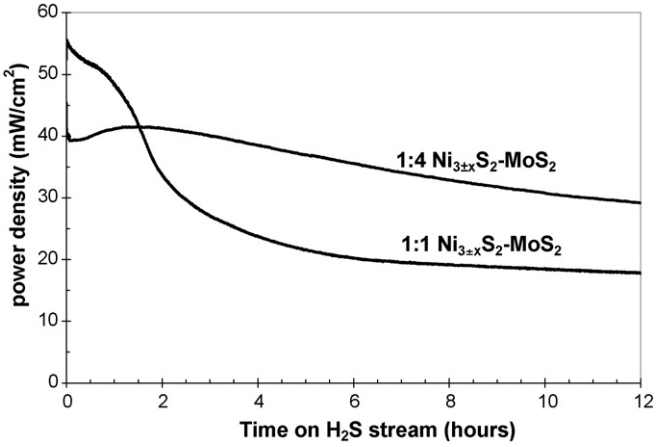

Fig. 6. Fuel cell power density as function of $Ni_{3\pm x}S_2$ content in composite anode at 800 °C.

of composite anodes with 1:1 and 1:2 ratios was almost half that of the two other ratios tested.

Fuel cell maximum current and power densities at 850 °C with various ratios of nickel sulfide to molybdenum sulfide are plotted in Fig. 5. The fuel cell employing the 1:1 anode achieved the highest current and power densities, 1350 mA cm^{-2} and 300 mW cm^{-2}, respectively, which is the best fuel cell performance obtained in SOFC using 100% H_2S feed. Electrochemical reactions taking place across electrode/electrolyte interfaces depend strongly on electrode processing parameters which may lead to morphological changes and cause fluctuations in performance. Although great efforts were made to control and keep all processing parameters consistent to ensure the reproducibility of all data, the performance results varied about 20% between experiments. Therefore, Fig. 5 presents fuel cell performance averaged over several tests performed with the same anode composition.

For successful commercial application of any anode material, its activity must be sustainable for a long period of use. The stability of the cells was tested in two modes, at OCV (zero current) and under polarization (fuel cell behavior). Later case is presented in Fig. 6 which shows the power densities as a function of time for the most active (1:1) and most stable (1:4) anode compositions at 800 °C. The cell with the 1:1 composition anode showed 66% decrease in power density over 12 h when compared with initial performance, and the cell with 1:4 anode composition showed stable performance over 3 h. After 3 h the performance slowly declined at about ca. 3.5% per hour, to an overall decrease of 27% after 12 h operation in a H_2S feed stream. Under OCV at 850 °C, the anode materials under investigation, except the catalyst with 1:4 weight ratio, showed degradation of performance within 4 h testing. The power density of the most active anode (1:1 weight ratio) decreased steadily by 45% during 4 h operation. Anode compositions with 1:2 ratio had a 38% decrease, and the 2:1 ratio anode had a 20% decrease over 4 h. EIS spectra clearly show that anode polarization resistance increased with time although R_s stayed almost the same.

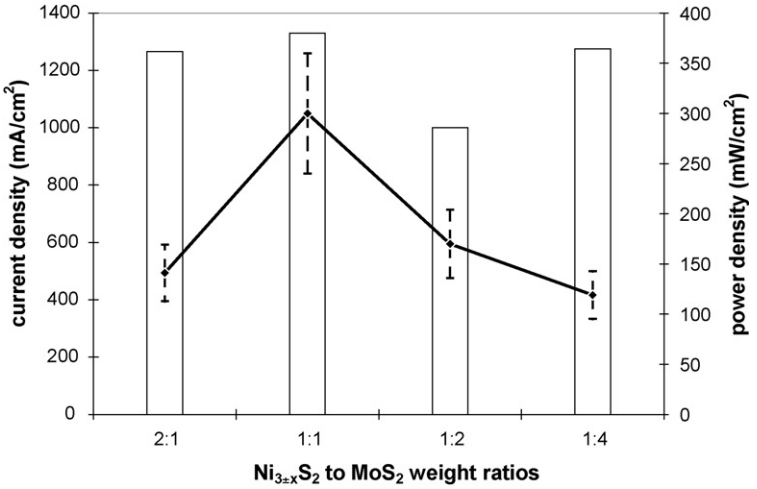

Fig. 5. Fuel cell performance of composite $Ni_{3\pm x}S_2$–MoS_2–Ag–YSZ anode at 850 °C (bars represent current density on the left and curve shows power density on the right).

3.4. The compositional and morphological changes of composite MoS_2–$Ni_{3\pm x}S_2$ anodes

SEM/EDX and NAA analyses were performed to determine the morphological and compositional changes of all anode compositions after the fuel cell tests. Table 1 shows results of NAA analysis of fresh and used samples. For each composition except 1:4, the relative amounts of Mo and Ni did not change during testing. The used anode with 1:4 ratio showed ca. 25% decrease in Mo content. These data indicate that there may be a minimum amount of $Ni_{3\pm x}S_2$ required to prevent oxidation/sublimation of MoS_2, which was not fulfilled by the 1:4 anode composition.

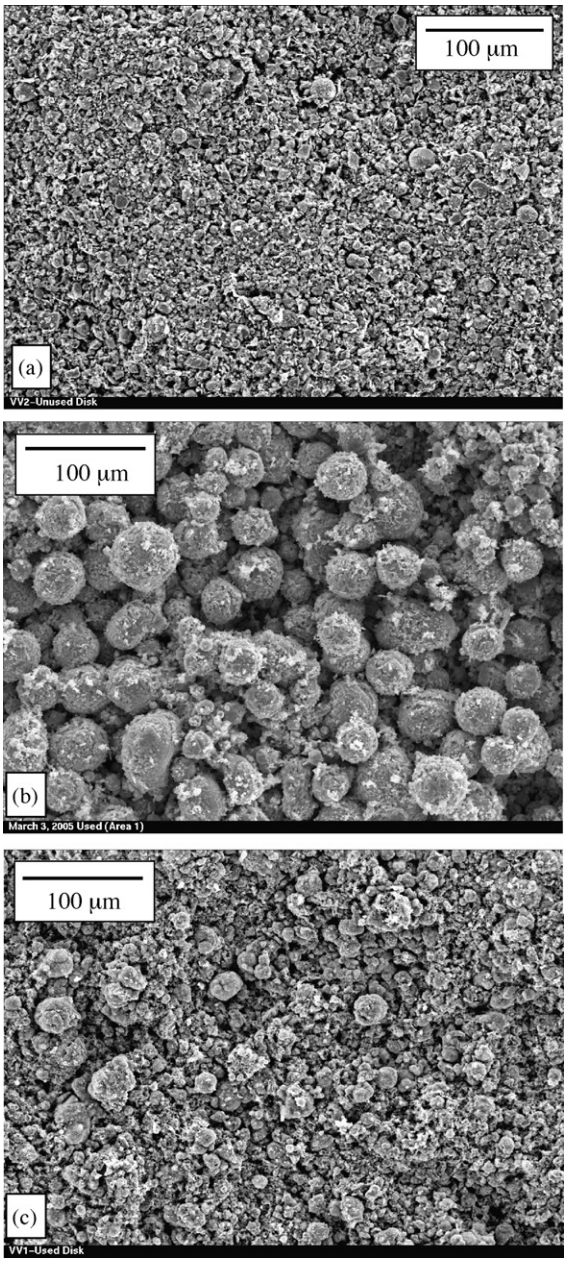

Fig. 7. SEM photograph of composite $Ni_{3\pm x}S_2$, MoS_2–Ag–YSZ anode with 1:1 weight ratio of nickel to molybdenum sulfide: (a) before fuel cell test, (b) after fuel cell test Ni-rich area (>75% is nickel sulfide) and (c) after fuel cell test Mo-rich area (>75% is molybdenum sulfide).

Our previous results have shown that there were no differences in phases between fresh and used samples [8].

EDX results for the anode after the fuel cell test revealed that there were areas rich (difference of 50% or more from the theoretical ratio of $Ni_{3\pm x}S_2$ to MoS_2) in either $Ni_{3\pm x}S_2$ or MoS_2 present within the used anode after the fuel cell tests, in contrast to more even distribution of $Ni_{3\pm x}S_2$ to MoS_2 components in fresh anodes (±5% from the theoretical $Ni_{3\pm x}S_2$ to MoS_2 ratio). Fig. 7 shows the SEM micrographs for the anode before and after fuel cell tests. Fig. 7(b) and (c) are the morphologies on the Ni-rich and Mo-rich areas, respectively. They show that the morphology changed significantly and the morphology was not uniform after the fuel cell tests. The SEM micrograph of the $Ni_{3\pm x}S_2$-rich area [Fig. 7 (b)] shows that nickel sulfide particles were strongly agglomerated after H_2S fuel cell tests and that agglomeration became more pronounced with time. Such agglomeration significantly reduced the catalytically active surface area of the nickel sulfide, and the reduction in number of active anode surface sites during fuel cell testing appeared to have caused the loss of electrochemical performance of the anode catalysts.

4. Conclusions

MoS_2 is thermally stable and non-volatile in N_2 up to 1000 °C. MoS_2 disappearance during fuel cell operation is due to its oxidation to MoO_3 which sublimated at temperatures above 600 °C.

Ni sulfide stabilizes Mo sulfide because addition of nickel sulfide to MoS_2 prevents the formation of MoO_3. However, a minimum amount of Ni must be present to ensure the formation of $NiMoO_4$ phase, rather than MoO_3.

All anode compositions with various ratios of nickel sulfide to molybdenum sulfide have high initial electrochemical activities for H_2S oxidation in SOFC. However, the performances of the anode materials for H_2S oxidation are not stable because of agglomeration of nickel sulfide particles and change in the anode composition.

Acknowledgments

Financial support from Shell Global Solutions is gratefully acknowledged. The authors would like to thank Dr. S. Duke, director of University of Alberta SLOWPOKE Nuclear Reactor Facility, for help with NAA analysis. Special thanks are to Dr. J. Melnik for very helpful discussions.

References

[1] N. Pujare, K. Tsai, A. Sammells, J. Electrochem. Soc. 136 (1989) 3662–3678.
[2] A.F. Sammells, J. Patel, J. Osborne, R.L. Cook, Gas Sep. Purif. 6 (3) (1992) 141–147.
[3] B.G. Ong, T.A. Lin, D.M. Mason, Electrochem. Soc. Proc. Ser. 12 (1987) 295–306.
[4] D. Weaver, J. Winnick, J. Electochem. Soc. 134 (1987) 2451–2458.
[5] C. Yates, J. Winnick, J. Electrochem. Soc. 146 (1999) 2841–2844.

[6] M. Liu, G. Wei, J. Luo, A.R. Sanger, K.T. Chuang, J. Electrochem. Soc. 150 (2003) A1025–A1029.
[7] M. Liu, H_2S-powered solid oxide fuel cells, PhD Thesis, University of Alberta, 2004.
[8] G. Wei, J. Luo, A.R. Sanger, K.T. Chuang, J. Electrochem. Soc. 151 (2004) A232–A237.
[9] M. Liu, P. He, J.L. Luo, A.R. Sanger, K.T. Chuang, J. Power Sources 94 (2001) 20–25.
[10] C.R. Hammond, in: D.R. Lide (Ed.), CRC Handbook of Chemistry and Physics, CRC Press, Inc., Boca Raton, 1992–1993, pp. 4–61.
[11] F. Jellinek, in: D.W.A. Sharp (Ed.), MTP International Review of Science: Inorganic Chemistry, series one, Butterworth, London, 1972, pp. 339–396.
[12] D. Weaver, J. Winnick, J. Electrochem. Soc. 138 (1991) 1626–1637.
[13] I.V. Yentekakis, C.G. Vayenas, J. Electrochem. Soc. 136 (1989) 996–1002.
[14] L. Aguilar, S. Zha, Z. Cheng, J. Winnick, M. Liu, J. Power Sources 135 (2004) 17–24.
[15] M. Liu, P. He, J. Luo, A.R. Sanger, K.T. Chuang, J. Power Sources 94 (2003) 20–25.
[16] T. Chivers, J.B. Hyne, C. Lau, Int. J. Hydrogen Energy 5 (1980) 499–506.
[17] K. Fukuda, M. Dokiya, T. Kameyama, Y. Kotera, Ind. Eng. Chem. Fundam. 17 (4) (1978) 243–248.
[18] P. Cannon, Nature 183 (1959) 1612–1613.
[19] S.K. Srivastava, B.N. Avasthi, J. Less-Common Met. 124 (1986) 85–92.
[20] G. Eckert, Werkst. Korros. 9 (1958) 69–72.
[21] L. Kolesnichenko, P. Trushko, L. Pugina, V. Ageeva, Poroshkovaya Metallurgiya 12 (7) (1972) 56–60.
[22] A. Zelikman, O. Krein, Zh. Fiz. Khim. 29 (1955) 2081–2085.
[23] Y. Shigegaki, S.K. Basu, M. Wakihara, M. Taniguchi, J. Therm. Anal. 34 (1988) 1427–1440.
[24] G.V. Samsonov, The Oxide Handbook, IFI/Plenum, New York, 1973, pp. 199–200.
[25] T. Kawada, H. Yokokawa, Key Eng. Mater. 125/126 (1997) 187–248.
[26] C.G. Vayenas, S. Ladas, S. Bebelis, I.V. Yentekakis, S. Neophytides, J. Yi, C. Karavasilis, C. Pliangos, Electrochim. Acta 39 (1994) 1849–1855.
[27] J.G. Dunn, C.E. Kelly, J. Therm. Anal. 12 (1977) 43–52.
[28] G.M. Mehrotra, V.B. Tare, J.B. Wagner Jr., J. Electrochem. Soc.: Solid State Sci. Technol. 132 (1) (1985) 244–247.
[29] T. Massalski, H. Okamoto, Binary Alloy Phase Diagrams, Second ed., ASM International, Materials Park, 1990, pp. 2852–2853.
[30] H. Kiuchi, K. Funaki, T. Tanaka, Metal. Trans. B 14B (1983) 347–352.